Inorganic Chemistry

pubs.acs.org/IC

Article

Crystal Structures and Property Measurements of Rare Earth Magnesium Thiosilicates Synthesized via Flux Crystal Growth Utilizing the Boron Chalcogen Mixture (BCM) Method

Adam A. King, Logan S. Breton, Greg Morrison, Mark D. Smith, Mingli Liang, P. Shiv Halasyamani, and Hans-Conrad zur Loye*

Cite This: *Inorg. Chem.* 2023, 62, 7446−7452

Read Online

ACCESS | Metrics & More | Article Recommendations | Supporting Information

ABSTRACT: Nine new rare earth magnesium-containing thiosilicates of the formula $RE_3Mg_{0.5}SiS_7$ (Ln = Ce, Pr, Nd, Sm, Gd, Tb, Dy, Ho, Er) were synthesized in an alkali halide flux using the boron chalcogen mixture (BCM) method. Crystals of high quality were produced, and their structures were determined by single-crystal X-ray diffraction. The compounds crystallize in the hexagonal crystal system in the $P6_3$ space group. Phase pure powders of the compounds were used for magnetic susceptibility measurements and for second-harmonic generation (SHG) measurements. Magnetic measurements indicate that $Ce_3Mg_{0.5}SiS_7$, $Sm_3Mg_{0.5}SiS_7$, and $Dy_3Mg_{0.5}SiS_7$ exhibit paramagnetic behavior with a negative Weiss temperature over the 2−300 K temperature range. SHG measurements of $La_3Mg_{0.5}SiS_7$ demonstrated SHG activity with an efficiency of 0.16 times the standard potassium dihydrogen phosphate (KDP).

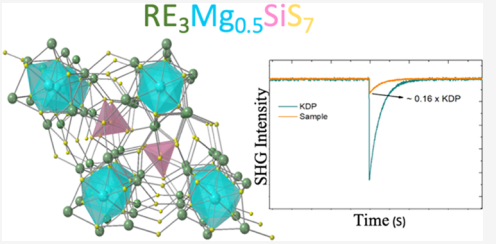

INTRODUCTION

Metal chalcogenides have become the foundation of many modern technologies due to their structural and compositional diversity, which results in a plethora of desired physical properties.[1] Chalcometallates, one class of chalcogenides, result from the combination of the chalcogens with certain main group elements that yield complex anionic framework structures. The zur Loye group, utilizing the molten flux synthetic method, has explored the synthesis of single crystals of a variety of chalcometallate materials, including thiophosphates, thiogermanates, and thiosilicates, to explore their magnetic and optical properties.[2,3] A major obstacle to the synthesis of these compounds is the lack of commercially available rare earth sulfide-starting materials, which necessitates their preparation in the laboratory prior to exploring the syntheses of chalcometallate compounds. Recently, we have demonstrated the use of the boron chalcogen mixture (BCM) method to synthesize single crystals of $LnBS_3$ (Ln = La, Ce, Pr, Nd) and measured their nonlinear optical properties.[4] The BCM method allows for the *in situ* sulfurization of lanthanide oxide starting reagents, thereby avoiding the need for lanthanide sulfide reagents.[5] As this method has been previously used to synthesize a number of lanthanide and transition metal sulfide compounds, we again chose to utilize the BCM method to explore a family of chalcometallates, $RE_3Mg_{0.5}SiS_7$ (RE = rare earth) compounds to investigate their magnetic and optical properties.[6−8]

The $RE_3M_xTQ_7$ (M = metal, T = Si, Ge) compounds represent an extensive family of quaternary rare-earth chalcogenides that due to the unique structural flexibility of the $La_3Mn_{0.5}GeS_7$ structure type can accommodate a variety of elements that can impart optical and magnetic properties to the material.[9−19] The structural flexibility of this family results from the metal atom's ability to have full occupancy and to take on a trigonal planar coordination environment, an example being La_3AgSiS_7, or be half occupied and take on an octahedral coordination environment, such as in $RE_3Cd_{0.5}GeS_7$.[20,21] The compositional flexibility stems from the wide variety of combinations of rare earths, metals, tetrels, and chalcogenides and consists of almost 2000 reported phases.[22] A survey of this family of compounds was recently published by Zhou et al., which highlighted the lack of certain elemental compositions within this phase space.[20] One series with minimal reported phases is the rare earth magnesium thiosilicates, $RE_3Mg_{0.5}SiS_7$, the $La_3Mg_{0.5}SiS_7$ and $Y_{0.5}Mg_{0.5}SiS_7$ analogues being the only ones reported.[23,24]

For this reason, we decided to investigate this series in order to explore the optical and magnetic properties of rare earth metals in various structural environments. Furthermore, Mg^{2+} is diamagnetic and optically inactive, enabling us to study solely the behavior of the rare earths in these compounds. Many of these compounds, including those presented in this

Received: March 3, 2023
Published: May 3, 2023

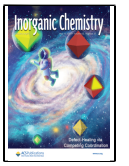

Downloaded via UNIV OF HOUSTON MAIN on August 17, 2023 at 15:55:25 (UTC).
See https://pubs.acs.org/sharingguidelines for options on how to legitimately share published articles.

ACS Publications

© 2023 American Chemical Society

Table 1. Crystallographic Data and Diffraction Results for All Reported Compounds

chemical formula	$La_3Mg_{0.5}SiS_7$	$Ce_3Mg_{0.5}SiS_7$	$Pr_3Mg_{0.5}SiS_7$	$Nd_3Mg_{0.5}SiS_7$	$Sm_3Mg_{0.5}SiS_7$
formula weight	681.40	685.03	687.40	697.39	715.79
crystal system	hexagonal				
space group, Z	$P6_3$	$P6_3$	$P6_3$	$P6_3$	$P6_3$
a, Å	10.35010(10)	10.23860(10)	10.18500(10)	10.1219(13)	10.03110(10)
c, Å	5.74220(10)	5.72220(10)	5.69630(10)	5.6691(11)	5.64820(10)
V, Å^3	532.719(14)	519.487(14)	511.735(13)	503.00(16)	492.195(13)
ρ_{calcd}, g/cm^3	4.248	4.379	4.461	4.605	4.829
radiation (λ, Å)	Mo Kα (0.710173 Å)				
μ, mm^{-1}	13.259	14.405	15.561	16.786	19.227
T, K	299.12	299.09	298.89	298.53	300.2
crystal dim., mm^3	0.04 × 0.04 × 0.04	0.05 × 0.05 × 0.04	0.05 × 0.05 × 0.05	0.05 × 0.05 × 0.05	0.05 × 0.05 × 0.05
2θ range, deg	3.938−36.302	2.297−36.259	4.001−36.302	2.323−36.326	2.344−36.341
reflections collected	22,794	22,771	22,302	22,801	21,059
data/parameters/restraints	1737/38/1	1683/38/1	1654/ 38 /1	1636/38/1	1589/38/1
R_{int}	0.0280	0.0280	0.0303	0.0356	0.0308
goodness of fit	1.165	1.211	1.193	1.132	1.234
$R_1(I > 2\sigma(I))$	0.0077	0.0097	0.0089	0.0085	0.0103
wR_2 (all data)	0.0179	0.0262	0.0206	0.0196	0.0236
Flack parameter	0.031(4)	0.027(5)	0.028(5)	0.023(5)	0.039(5)
chemical formula	$Gd_3Mg_{0.5}SiS_7$	$Tb_3Mg_{0.5}SiS_7$	$Dy_3Mg_{0.5}SiS_7$	$Ho_3Mg_{0.5}SiS_7$	$Er_3Mg_{0.5}SiS_7$
formula weight	736.42	741.43	752.17	759.46	766.45
crystal system	hexagonal				
space group, Z	$P6_3$	$P6_3$	$P6_3$	$P6_3$	$P6_3$
a, Å	9.9571(3)	9.8952(5)	9.84310(10)	9.7890(11)	9.75330(10)
c, Å	5.6344(3)	5.6257(4)	5.62710(10)	5.6255(9)	5.63680(10)
V, Å^3	483.78(4)	477.04(6)	472.149(13)	466.84(13)	464.372(13)
ρ_{calcd}, g/cm^3	5.055	5.162	5.291	5.403	5.481
radiation (λ, Å)	Mo Kα (0.710173 Å)				
μ, mm^{-1}	21.918	23.611	25.126	26.826	28.519
T, K	303(2)	299.74	303(2)	297.69	299.32
crystal dim., mm^3	0.06 × 0.06 × 0.04	0.05 × 0.05 × 0.05	0.07 × 0.06 × 0.04	0.04 × 0.04 × 0.04	0.05 × 0.05 × 0.04
2θ range, deg	2.362−40.290	2.377−36.315	2.389−40.265	2.402−36.287	2.411−36.325
reflections collected	29,133	19,488	30,408	20,237	19,302
data/parameters/restraints	2028/38/1	1536/38/1	1998/37/1	1507/38/1	1498/38/1
R_{int}	0.0322	0.0316	0.0324	0.0335	0.0319
goodness of fit	1.160	1.232	1.25	1.194	1.224
$R_1(I > 2\sigma(I))$	0.0101	0.0095	0.0112	0.0096	0.0118
wR_2 (all data)	0.0214	0.0229	0.0227	0.0215	0.0270
Flack parameter	0.026(8)	0.043(5)	0.025(8)	0.036(4)	0.059(5)

paper, crystallize in the noncentrosymmetric space group $P6_3$, which makes these structures potentially SHG active and, thus, able to exhibit nonlinear optical properties (NLO). To date, the synthesis of the known $RE_3M_xTQ_7$ (M = metal, T = Si, Ge) compounds has primarily been carried out by solid-state syntheses, although a few other synthetic routes have been reported, such as molten flux synthesis and arc melting of precursors.[25,26] We chose to utilize the combined BCM and molten flux methods to grow crystals of the title compounds for structural characterization and, in some cases, also performed solid-state synthesis using the BCM method to create bulk samples. Herein, we present the synthesis of high-quality single crystals of $RE_3Mg_{0.5}SiS_7$ (RE = La-Nd, Sm-Er) and the determination of their crystal structures. Furthermore, the magnetic properties of $RE_3Mg_{0.5}SiS_7$ (Ce, Dy, Sm) are investigated and the SHG properties of $La_3Mg_{0.5}SiS_7$ are reinvestigated.

EXPERIMENTAL SECTION

RE_2O_3 (RE = La, Nd, Sm, Gd, Dy, Ho, Er) (99.9%, Alfa Aesar), CeO_2 (99.9%, Alfa Aesar), Pr_6O_{11} (99.9% Alfa Aesar), Tb_4O_7 (99.9% Alfa Aesar), sulfur (Fischer Scientific), boron (crystalline 100 mesh, 99.9%, Beantown Chemical), SiO_2 (amorphous powder, 99.9%, Alfa Aesar), NaI (99.9%, Beantown Chemical), NaCl (99.9%, Alfa Aesar), $CaCl_2$ (Fisher Scientific), and $MgCO_3$ (Allied Chemicals) reagents were used to synthesize the target compounds. MgO was prepared by decomposing $MgCO_3$ at 700 °C for 24 h. Pr_2O_3 and Tb_2O_3 were prepared by the reduction of Pr_6O_{11} and Tb_4O_7 at 1000 °C for 24 h under a 4% hydrogen flow. The resulting Tb_2O_3 and Pr_2O_3 were stored in a nitrogen glovebag. NaI, NaCl, $CaCl_2$, and MgO were stored overnight in a drying oven set to 260 °C to remove moisture.

$RE_3Mg_{0.5}SiS_7$ (RE = Nd-Er) were synthesized by the addition of 50 mg of RE_2O_3, 10 mg of boron, 45 mg of sulfur, 5 mg of SiO_2, and 2 mg of MgO powders into a fused silica tube (10 mm × 12 mm inner and outer diameters, about 15 cm length) along with 250 mg of NaI flux (75 mg in the case of Nd). The fused silica tube was evacuated to 10^{-4} torr and flame-sealed using a methane/oxygen torch. The sealed fused silica tube was placed into a programmable furnace set to heat to 760 °C in 20 h to dwell at this temperature for 20 h and to cool to

https://doi.org/10.1021/acs.inorgchem.3c00708
Inorg. Chem. 2023, 62, 7446−7452

560 °C in 20 h, at which point the furnace was shut off and allowed to return to room temperature.

$RE_3Mg_{0.5}SiS_7$ (RE = La, Pr) were synthesized using a similar procedure, except for the use of 75 mg of a $CaCl_2$/NaCl eutectic instead of NaI, and the reagent mixture was ground using a mortar and pestle prior to the addition of the flux. The tube was heated to 950 °C in 20 h, dwelled at this temperature for 20 h, and cooled to 750 °C in 20 h, at which point the furnace was shut off and allowed to return to room temperature.

$RE_3Mg_{0.5}SiS_7$ (RE = Ce) was obtained using the same synthetic procedures as the RE = La and Pr analogues but with the use of 75 mg of NaCl flux instead of the $CaCl_2$/NaCl eutectic.

To prepare samples for property measurements of $RE_3Mg_{0.5}SiS_7$ (RE = La-Sm), solid-state syntheses were performed using the BCM method, and the same materials were used for the flux reactions, however, with the absence of the flux. The masses used were also consistent with the masses mentioned above. For these reactions, the reagents were intimately ground. The ground mixture was added to a fused silica tube that was placed into a programmable furnace set to ramp to 950°C and dwelled for 12 h, at which point the furnace was shut off and allowed to return to room temperature.

Methanol was initially used for the dissolution of the flux, however, impurities in the product remained. For that reason, water was used for the workup after establishing that the target compositions are sufficiently air and water stable. This successfully removed the impurity phases from the later rare earths (RE = Gd-Er). The powder X-ray diffraction patterns of all materials used for property measurements can be seen in Figures S1−S4.

Caution. Boron sulfides are moisture-sensitive and produce H_2S gas in contact with moisture and water. All reaction work needs to be performed in fume hoods with the proper safety procedures in place.

Single-Crystal X-ray Diffraction (SXRD). X-ray intensity data of yellowish−brown plate crystals of all title compositions were collected at 300 K using a Bruker D8 QUEST diffractometer equipped with a PHOTON-II area detector and an Incoatec microfocus source (Mo Kα radiation, λ = 0.71073 Å). Single crystals were mounted on a microloop with immersion oil. The raw area detector data frames were reduced and corrected for absorption effects using the SAINT+ and SADABS programs.[27] Final unit cell parameters were determined by the least-squares refinement of a large array of reflections from each data set.[28] An initial structural model was obtained with SHELXT. Subsequent difference Fourier calculations and full-matrix least-squares refinement against F^2 were performed with SHELXL-2018 using the ShelXle interface.[29] All compounds crystalize in the noncentrosymmetric, hexagonal space group $P6_3$. The asymmetric unit contains three sulfur atoms, one lanthanide atom, one magnesium atom, and one silicon atom. All atoms are all located in positions of general crystallographic symmetry. All atoms were refined with anisotropic displacement parameters. The Mg occupancy refined in all cases to ∼0.5 within standard deviation (0.497(5) for $Nd_3Mg_{0.5}SiS_7$) and was therefore fixed at 0.5. The crystallographic data and diffraction results are listed in Table 1.

Powder X-ray Diffraction (PXRD). Powder X-ray diffraction (PXRD) data were collected using a powder sample of $RE_3Mg_{0.5}SiS_7$ obtained by the solid-state synthesis (Figures S1−S4). Data were collected on a Bruker D2 PHASER diffractometer using Cu Kα radiation over a 2θ range 10−65° with a step size of 0.02°.

Magnetic Susceptibility. Magnetic property measurements of $Ce_3Mg_{0.5}SiS_7$, $Sm_3Mg_{0.5}SiS_7$, and $Dy_3Mg_{0.5}SiS_7$ were performed using a Quantum Design magnetic property measurement system (QD MPMS 3 SQUID Magnetometer). The magnetic susceptibility was measured under zero-field-cooled (zfc) and field-cooled (fc) conditions from 2 to 300 K in an applied magnetic field of 0.1 T. Magnetization as a function of the applied field was measured from −5 to 5 T at 2 K. Data were corrected for the sample shape and radial offset effects as described previously.[30]

UV−Vis Diffuse Reflectance Spectroscopy. UV−vis diffuse reflectance data, 300−900 nm, for $La_3Mg_{0.5}SiS_7$ were obtained using a PerkinElmer Lambda 35 UV−vis scanning spectrophotometer equipped with an integrating sphere. The reflectance data were converted to absorbance using the Kubelka−Munk function.[31]

Second-Harmonic Generation (SHG). The Kurtz−Perry method was adopted to assess the SHG performance of the sample. Polycrystalline powder of the sample was placed in the tubes of quartz and then irradiated with a pulsed infrared beam (1064 nm) produced by a Q-switched Nd:YAG laser. The generated second-harmonic signals (532 nm) were collected by the detector. KDP (KH_2PO_4) served as a standard during the SHG test procedure.[32,33]

RESULTS AND DISCUSSION

Synthesis. A review of $RE_3M_xTQ_7$ compounds reveals that a significant number of compositions that are structurally and compositionally related to $RE_3M_xTQ_7$, and that are of interest for better understanding of the crystal chemistry of thiosilicates, have not been reported. We targeted the synthesis of some of these compositions to investigate their crystal chemistry and, at the same time, to extend the use of our BCM method to more diverse structural families. Therefore, we used the BCM method to synthesize the $RE_3Mg_{0.5}SiS_7$ family both as powders and as single crystals. Table 2 lists the known compositions of the $Ln_3Mg_{0.5}SiS_7$ structure type, while Table 3 lists the known compositions of the $Ln_3Mg_{0.5}GeS_7$ structure type; clearly, more thiogermanates than thiosilicates have been reported.

Table 2. Known Thiosilicate Compounds of the $RE_3Mg_{0.5}SiS_7$ Series[a]

	Ln^{3+}										
M^{2+}	La	Ce	Pr	Nd	Sm	Gd	Tb	Dy	Ho	Er	ref
Mg	•										23, 24
Cr	•										22, 23
Mn	•	•	•	•	•	•		•		•	9, 22, 23
Fe	•				•						18, 22, 23
Co	•										15, 22
Ni	•										15, 22
Zn	•	•	•	•	•	•	•	•	•	•	20
Cd	•	•	•	•	•	•	•	•	•		20

[a]•-Reported compound.

Table 3. Known Thiogermanate Compounds of the $RE_3Mg_{0.5}GeS_7$ Series[a]

	Ln^{3+}										
M^{2+}	La	Ce	Pr	Nd	Sm	Gd	Tb	Dy	Ho	Er	ref
Mg	•	•	•	•	•	•	•	•	•	•	13, 24
Cr	•										23
Mn	•	•	•	•	•	•	•	•	•	•	11, 23
Fe	•	•	•	•	•	•	•	•	•	•	10
Co	•	•	•	•	•	•	•	•	•	•	12, 14
Ni	•	•	•	•	•	•	•	•	•	•	12, 14
Zn	•	•	•	•	•	•	•	•	•	•	20
Cd	•	•	•	•	•	•	•	•			20

[a]•-Reported compound.

We performed the synthesis of $RE_3Mg_{0.5}SiS_7$ RE = La, Ce, Pr, Nd, Sm-Er series, targeting both single crystals and powders. Using NaI (Nd, Sm-Er) and $CaCl_2$/NaCl (La, Ce, Pr) as fluxes and using boron powder to remove the oxygen from our RE_2O_3 reagents, we successfully obtained high-quality single crystals for all of the target compositions. Although the

https://doi.org/10.1021/acs.inorgchem.3c00708
Inorg. Chem. 2023, 62, 7446−7452

RE = Sm-Er target phases were crystallized as the major product, $Mg_2(SiS_4)$ was identified as a minor impurity phase in these reactions and, even after numerous attempts to optimize the flux crystal growth reaction conditions, could not be eliminated. For RE = La-Nd, the target phases would not form when using the same synthetic procedure used to obtain the RE = Sm-Er compounds due to the formation of $RE_3(SiS_4)_2I$ as the major reaction product.[34] It is important to note that while $Sm_3(SiS_4)_2I$ has been reported, the chlorine analogue has not.[35] This may be the reason why the NaI flux led to the formation of $Sm_3(SiS_4)_2I$, while the chloride flux did not, vide infra, form $Sm_3(SiS_4)_2Cl$. To eliminate the $RE_3(SiS_4)_2I$ phases entirely from the product, the NaI flux was changed to the $NaCl/CaCl_2$ eutectic. This led to the successful synthesis of the target phases, $La_3Mg_{0.5}SiS_7$ and $Pr_3Mg_{0.5}SiS_7$, which formed as minor products along with a new rare earth calcium-containing thiosilicate as the major product. We will report on the latter materials in the near future. To eliminate the formation of this calcium-containing phase for the synthesis of the cerium and neodymium phases, a NaCl flux was used. The target phase, $Ce_3Mg_{0.5}SiS_7$, was successfully synthesized using this method. The target phase, $Nd_3Mg_{0.5}SiS_7$, was synthesized by decreasing the flux amount from 200 to 75 mg. Attempts at the synthesis of RE = Tm-Lu using the synthetic routes described above failed. In all cases, only $MgRE_2S_4$ and $Mg_2(SiS_4)$ were isolated. This is perhaps not unexpected as no other RE-Mg-Si-S compositions belonging to this structure type have been reported, as illustrated in Table 2.

Structure Description. The $RE_3Mg_{0.5}SiS_7$ structure is a member of the $RE_3M_{0.5}TQ_7$ family of compounds that crystallizes in the hexagonal crystal system, adopting the noncentrosymmetric space group $P6_3$. All of the title compositions are isostructural and crystallize in this space group. This three-dimensional structure consists of RES_8 bi-capped trigonal prisms that edge and corner share to create a ring-like assembly. Isolated SiS_4 tetrahedra throughout the structure are located between each ring-like assembly of RES_8 bi-capped trigonal prisms. Face-sharing MgS_6 octahedra are located in the middle of the ring-like assembly. Figure 1 illustrates the local coordination environments of the RE^{3+}, Si^{4+}, and Mg^{2+} cations, respectively, along with the general structure of $RE_3Mg_{0.5}SiS_7$. Figure 2 contains a plot of the unit cell volume of $RE_3Mg_{0.5}SiS_7$ as a function of the rare-earth ionic radius. The decrease in volume when going from La to Er is expected due to the lanthanide contraction in these compounds.

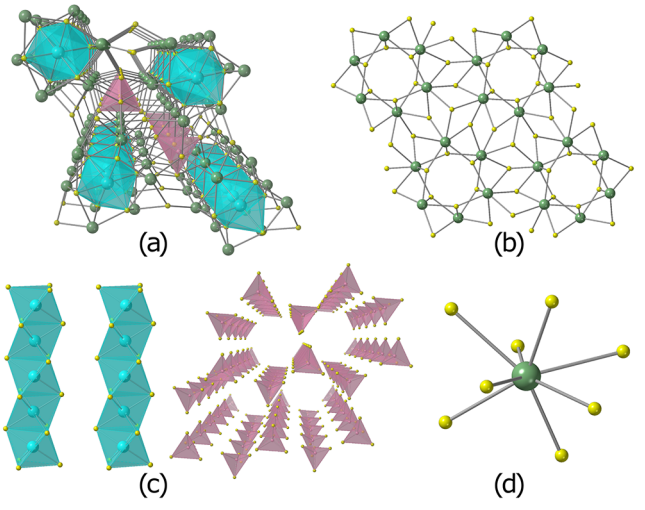

Figure 1. (a) Three-dimensional (3D) framework structure of $Gd_3Mg_{0.5}SiS_7$ viewed down the *c*-direction. (b) GdS_8 chains developing the framework. (c) Face-sharing MgS_6 octahedra and isolated SiS_4 tetrahedra. (d) Gd coordination environment.

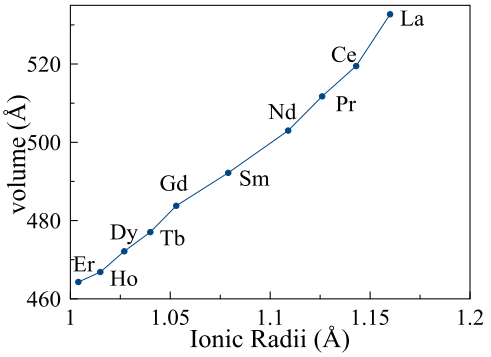

Figure 2. Volume vs ionic radii of the RE^{3+} elements in the $RE_3Mg_{0.5}SiS_7$ structure.

Magnetic Properties. The magnetic susceptibility data for $Ce_3Mg_{0.5}SiS_7$, $Dy_3Mg_{0.5}SiS_7$, and $Sm_3Mg_{0.5}SiS_7$ are shown in Figure 3. The data in these plots were analyzed and the magnetic moment was extracted from a fit to the Curie–Weiss Law. The moments and Weiss constants are summarized in Table 4 and were found to be in excellent agreement with the calculated moments. The negative Weiss temperatures suggest antiferromagnetic interactions, but as seen in Figure 3, no antiferromagnetic transitions are observed above 2 K, the lowest temperature measured.

The Samarium analogue, as expected, exhibits Van Vleck paramagnetism in the 2–300 K temperature range measured.[36] Due to the lack of Curie–Weiss behavior, the effective moment of Sm^{3+} at room temperature was determined to be 1.45 μ_B/Sm^{3+}. This is in agreement with other Sm chalcogenides, such as the reported $BaSm_2S_4$, which has an experimentally reported moment of 1.47 μ_B/Sm^{3+}.[37]

Optical Properties. UV–vis diffuse reflectance data were collected on the $La_3Mg_{0.5}SiS_7$ sample. A Tauc plot indicates that $La_3Mg_{0.5}SiS_7$ is a direct band gap semiconductor with a band gap of 2.77 eV (Figure S5). In addition, $La_3Mg_{0.5}SiS_7$ was examined for SHG behavior. Materials that crystallize in a noncentrosymmetric crystal class may exhibit SHG behavior,[36] and a multitude of reported $RE_3M_xTQ_7$ compositions that crystallize in the noncentrosymmetric space group $P6_3$ have had their SHG properties analyzed.[38,39] La_3LiTS_7 (T = Ge, Sn) exhibits a strong NLO effect and high laser damage threshold (LDT), likely caused by a mixed contribution of LnS_8 and TS_4 groups.[40] We decided to investigate the SHG properties of $La_3Mg_{0.5}SiS_7$, which had been reported as SHG inactive.[24] Measurements on our $La_3Mg_{0.5}SiS_7$ sample indicated that it was in fact SHG active with an efficiency of ~0.16 times the standard KDP. Figure 4 shows the SHG intensity vs time of $La_3Mg_{0.5}SiS_7$ and the KDP standard. Due to the coloration of the crystals of the other compositions that interferes with SHG measurements, no other samples were tested for SHG activity.

https://doi.org/10.1021/acs.inorgchem.3c00708
Inorg. Chem. 2023, 62, 7446–7452

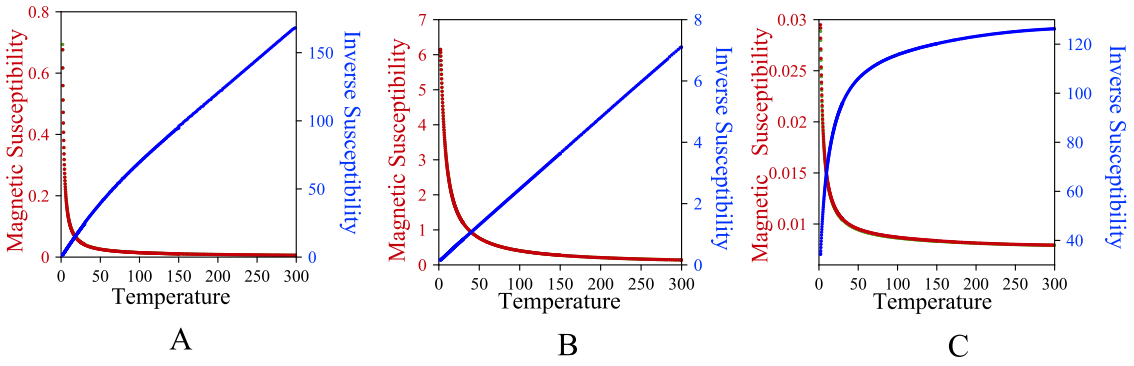

Figure 3. Susceptibility and inverse susceptibility vs temperature plots for $Ce_3Mg_{0.5}SiS_7$ (A), $Dy_3Mg_{0.5}SiS_7$ (B), and $Sm_3Mg_{0.5}SiS_7$ (C).

Table 4. Magnetic Data for $Ce_3Mg_{0.5}SiS_7$ AND $Dy_3Mg_{0.5}SiS_7$

compound	observed μ_{eff} (μ_B/Ln^{3+}) from Curie–Weiss fit (200–300 K)	calculated μ_{eff} (μ_B/Ln^{3+})	Θ_W (K)
$Ce_3Mg_{0.5}SiS_7$	2.33	2.54	−43.7
$Dy_3Mg_{0.5}SiS_7$	10.67	10.65	−5.4

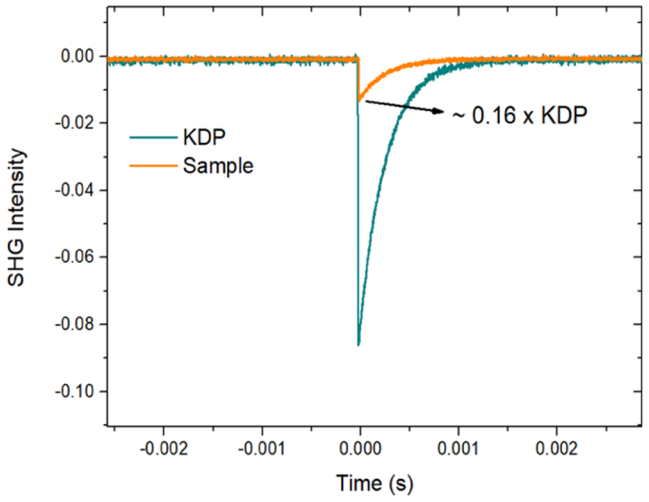

Figure 4. SHG intensity vs time of sample and KDP.

CONCLUSIONS

In this paper, we report the successful synthesis and structure determination of nine new members of the $RE_3Mg_{0.5}SiS_7$ series, $RE_3Mg_{0.5}SiS_7$ (RE = La-Nd, Sm-Er), representing an addition to the larger $RE_3M_{0.5}TQ_7$ family of compounds. By combining the BCM method and molten flux crystal growth, we succeeded in preparing high-quality single crystals of $RE_3Mg_{0.5}SiS_7$ (RE = La-Nd, Sm-Er) using binary oxides as starting reagents. In addition, we combined the BCM method with solid-state synthesis to prepare phase pure polycrystalline powders for property measurements. Due to the non-centrosymmetry of the crystal structures, SHG behavior of the $La_3Mg_{0.5}SiS_7$ compound was measured, establishing that this compound is SHG active with an intensity of 0.16 × KDP. Magnetic susceptibility measurements showed that $Ce_3Mg_{0.5}SiS_7$, $Dy_3Mg_{0.5}SiS_7$, and $Sm_3Mg_{0.5}SiS_7$, exhibit paramagnetic behavior with no obvious magnetic transition down to 2 K.

The BCM method is a valuable tool in metal chalcogenide synthesis as it provides more facile access to chalcogenide materials due to the ability to use commercially readily available oxide reagents as starting materials. As a result, the method can be used to synthesize a wide variety of new compositions in single crystal form. As the BCM method is still relatively new, we are in the process of expanding the BCM method to related thiosilicate compositions in order to also explore their physical properties.

ASSOCIATED CONTENT

Supporting Information

The Supporting Information is available free of charge at https://pubs.acs.org/doi/10.1021/acs.inorgchem.3c00708.

Powder X-ray diffraction patterns of $La_3Mg_{0.5}SiS_7$, $Ce_3Mg_{0.5}SiS_7$, $Sm_3Mg_{0.5}SiS_7$, and $Dy_3Mg_{0.5}SiS_7$; Tauc plot of $La_3Mg_{0.5}SiS_7$ (PDF)

(PDF)

Accession Codes

CCDC 2242918–2242924, 2243374–2243375, and 2248683 contain the supplementary crystallographic data for this paper. These data can be obtained free of charge via www.ccdc.cam.ac.uk/data_request/cif, or by emailing data_request@ccdc.cam.ac.uk, or by contacting The Cambridge Crystallographic Data Centre, 12 Union Road, Cambridge CB2 1EZ, UK; fax: +44 1223 336033.

AUTHOR INFORMATION

Corresponding Author

Hans-Conrad zur Loye − *Department of Chemistry and Biochemistry, University of South Carolina, Columbia, South Carolina 29208, United States;* orcid.org/0000-0001-7351-9098; Email: zurloye@mailbox.sc.edu

Authors

Adam A. King − *Department of Chemistry and Biochemistry, University of South Carolina, Columbia, South Carolina 29208, United States*

Logan S. Breton − *Department of Chemistry and Biochemistry, University of South Carolina, Columbia, South Carolina 29208, United States*

Greg Morrison − *Department of Chemistry and Biochemistry, University of South Carolina, Columbia, South Carolina 29208, United States;* orcid.org/0000-0001-9674-9224

Mark D. Smith − *Department of Chemistry and Biochemistry, University of South Carolina, Columbia, South Carolina 29208, United States*

Mingli Liang − *Department of Chemistry, University of Houston, Houston, Texas 77204-5003, United States*

https://doi.org/10.1021/acs.inorgchem.3c00708
Inorg. Chem. 2023, 62, 7446−7452

P. Shiv Halasyamani − *Department of Chemistry, University of Houston, Houston, Texas 77204-5003, United States*

Complete contact information is available at: https://pubs.acs.org/10.1021/acs.inorgchem.3c00708

Notes

The authors declare no competing financial interest.

■ ACKNOWLEDGMENTS

Research was supported by the U.S. Department of Energy, Office of Basic Energy Sciences, Division of Materials Sciences and Engineering under award DE-SC0018739. Synthesis, structural characterization, and magnetic studies performed at UofSC. SHG measurements performed at the University of Houston were supported by NSF DMR-2002319.

■ REFERENCES

(1) Kanatzidis, M. G. Discovery-Synthesis, Design, and Prediction of Chalcogenide Phases. *Inorg. Chem.* **2017**, *56*, 3158−3173.
(2) Breton, L. S.; Smith, M. D.; zur Loye, H.-C. Trends in Rare Earth Thiophosphate Syntheses: $Rb_3Ln(PS_4)_2$ (Ln = La, Ce, Pr), $Rb_{3-x}Na_xLn(PS_4)_2$ (Ln = Ce, Pr; x = 0.50, 0.55), and RbEu-PS_4Obtained by Molten Flux Crystal Growth. *CrystEngComm* **2021**, *23*, 5241−5248.
(3) Usman, M.; Smith, M. D.; Morrison, G.; Klepov, V. V.; Zhang, W.; Halasyamani, P. S.; zur Loye, H.-C. Molten Alkali Halide Flux Growth of an Extensive Family of Noncentrosymmetric Rare Earth Sulfides: Structure and Magnetic and Optical (SHG) Properties. *Inorg. Chem.* **2019**, *58*, 8541−8550.
(4) Breton, L. S.; Morrison, G.; Lacroix, M. R.; Halasyamani, P. S.; zur Loye, H.-C. Lanthanide thioborates, an emerging class of nonlinear optical materials, efficiently synthesized using the boron-chalcogen mixture method. *Chem. Commun.* **2022**, *58*, 7992−7995.
(5) Breton, L. S.; Klepov, V. V.; zur Loye, H.-C. Facile Oxide to Chalcogenide Conversion for Actinides Using the Boron-Chalcogen Mixture Method. *J Am. Chem. Soc.* **2020**, *142*, 14365−14373.
(6) Wu, L.-M.; Seo, D. K. New solid-gas metathetical synthesis of binary metal polysulfides and sulfides at intermediate temperatures: utilization of boron sulfides. *J. Am. Chem. Soc.* **2004**, *126*, 4676−4681.
(7) Huang, Y.-Z.; Chen, L.; Wu, L.-M. Crystalline Nanowires of Ln_2O_2S, $Ln_2O_2S_2$, LnS_2 (Ln = La, Nd), and $La_2O_2S:Eu^{3+}$. Conversions via the Boron-Sulfur Method That Preserve Shape. *Cryst. Growth Des.* **2008**, *8*, 739−743.
(8) Huang, Y.-Z.; Chen, L.; Wu, L.-M. Submicrosized rods, cables, and tubes of ZnE (E = S, Se, Te): exterior-interior boron-chalcogen conversions and optical properties. *Inorg. Chem.* **2008**, *47*, 10723−10728.
(9) Collin, G.; Laruelle, P. Structure de $La_6Cu_2Si_2S_{14}$. *Bull. Soc. Fr. Mineral. Cristallogr.* **1971**, *94*, 175−176.
(10) Daszkiewicz, M.; Pashynska, Y. O.; Marchuk, O. V.; Gulay, L. D.; Kaczorowski, D. Crystal structure and magnetic properties of $R_3Fe_{0.5}GeS_7$ (R = Y, La, Ce, Pr, Sm, Gd, Tb, Dy, Ho, Er and Tm). *J. Alloys Compd.* **2014**, *616*, 243−249.
(11) Daszkiewicz, M.; Marchuk, O. V.; Gulay, L. D.; Kaczorowski, D. Crystal structure and magnetic properties of $R_3Mn_{0.5}GeS_7$ (R=Y, Ce, Pr, Nd, Sm, Gd, Tb, Dy, Ho and Er). *J. Alloys Compd.* **2014**, *610*, 258−263.
(12) Daszkiewicz, M.; Pashynska, Y. O.; Marchuk, O. V.; Gulay, L. D.; Kaczorowski, D. Crystal structure and magnetic properties of $R_3Co_{0.5}GeS_7$ (R = Y, La, Ce, Pr, Nd, Sm, Gd, Tb, Dy, Ho, Er and Tm) and $R_3Ni_{0.5}GeS_7$(R = Y, Ce, Sm, Gd, Tb, Dy, Ho, Er and Tm). *J Alloys Compd.* **2015**, *647*, 445−455.
(13) Huch, M. R.; Gulay, L. D.; Olekseyuk, I. D. Crystal structures of the $R_3Mg_{0.5}GeS_7$ (R=Y, Ce, Pr, Nd, Sm, Gd, Tb, Dy, Ho and Er) compounds. *J Alloys Compd.* **2006**, *424*, 114−118.
(14) Iyer, A. K.; Yin, W.; Lee, E. J.; Lin, X.; Mar, A. Quaternary rare-earth sulfides $RE_3M_{0.5}GeS_7$ (RE=La−Nd, Sm; M=Co, Ni) and $Y_3Pd_{0.5}SiS_7$. *J. Solid State Chem.* **2017**, *250*, 14−23.
(15) Jin, Z.; Li, Z.; Du, Y. Synthesis and the crystal structure of $La_6NiSi_2S_{14}$ and $La_6CoSi_2S_{14}$. *Yingyong Huaxue* **1985**, *2*, 42−46.
(16) Michelet, A.; Flahaut, J. Sur les composés du type $La_6MnSi_2S_{14}$. *C. R. Acad. Sci., Ser. C.* **1969**, *269*, 1203−1205.
(17) Strok, O.; Daszkiewicz, M.; Gulay, L. Crystal structure of $R_3Mg_{0.5}DSe_7$ (*R* = Ce, Pr; *D* = Si, Ge). Chem. *Met. Alloys.* **2015**, *8*, 16−21.
(18) Sun, Y.-L.; Yang, C.; Guo, S.-P. Synthesis and crystal structure of a new quaternary sulfide $FeSm_6Si_2S_{14}$. *Jiegou Huaxue* **2013**, *202*, 269−275.
(19) Yin, W.; Wang, W.; Kang, L.; Lin, Z.; Feng, K.; Shi, Y.; Hao, W.; Yao, J.; Wu, Y. Ln_3FeGaQ_7: A new series of transition-metal rare-earth chalcogenides. *J. Solid State Chem.* **2013**, *202*, 269−275.
(20) Zhou, Y.; Iyer, A. K.; Oliynyk, A. O.; Heyberger, M.; Lin, Y.; Qiu, Y.; Mar, A. O.-H. Quaternary rare-earth sulfides $RE_3M_{0.5}M'S_7$ (M = Zn, Cd; M′ = Si, Ge). *J. Solid State Chem.* **2019**, *278*, No. 120914.
(21) Wu, L.-B.; Huang, F.-Q. Crystal structure of trilanthanum monosilver monosilicon heptasulfide, La_3AgSiS_7. *Z. Kristallogr. - New Cryst. Struct.* **2005**, *220*, 327−328.
(22) Akopov, G.; Hewage, N. W.; Yox, P.; Viswanathan, G.; Lee, S. J.; Hulsebosch, L. P.; Cady, S. D.; Paterson, A. L.; Perras, F. A.; Xu, W.; Wu, K.; Mudryk, Y.; Kovnir, K. Synthesis-enabled exploration of chiral and polar multivalent quaternary sulfides. *Chem. Sci. J.* **2021**, *12*, 14718−14730.
(23) Collin, G.; Laruelle, P. Structure cristalline de $La_6MnSi_2S_{14}$. *C. R. Acad. Sci., Ser. C.* **1970**, *270*, 410−412.
(24) Gitzendanner, R. L.; Spencer, C. M.; DiSalvo, F. J.; Pell, M. A.; Ibers, J. A. Synthesis and Structure of a New Quaternary Rare-Earth Sulfide, $La_6MgGe_2S_{14}$, and the Related Compound $La_6MgSi_2S_{14}$. *J. Solid State Chem.* **1997**, *131*, 399−404.
(25) Lin, F.; Luo, M.; Wang, R.; Che, X.; Huang, F. $La_6Cd_{0.75}Ga_2Q_{11.5}Cl_{2.5}$ (Q = S and Se): two new nonlinear optical chalcohalides with a large laser-induced damage threshold. *CrystEng-Comm* **2021**, *23*, 2133−2137.
(26) He, J.; Wang, Z.; Zhang, X.; Cheng, Y.; Gong, Y.; Lai, X.; Zheng, C.; Lin, J.; Huang, F. Synthesis, structure, magnetic and photoelectric properties of $Ln_3M_{0.5}M'Se_7$ (Ln = La, Ce, Sm; M = Fe, Mn; M′ = Si, Ge) and $La_3MnGaSe_7$. *RSC Adv.* **2015**, *5*, 52629−52635.
(27) Krause, L.; Herbst-Irmer, R.; Sheldrick, G. M.; Stalke, D. Comparison of silver and molybdenum microfocus X-ray sources for single-crystal structure determination. *J. Appl. Crystallogr.* **2015**, *48*, 3−10.
(28) Sheldrick, G. M. *Shelxt*− Integrated Space-Group and Crystal-Structure Determination. *Acta Crystallogr., Sect. A: Found. Adv.* **2015**, *71*, 3−8.
(29) Hübschle, C. B.; Sheldrick, G. M.; Dittrich, B. ShelXle: a Qt graphical user interface for SHELXL. *J Appl. Crystallogr.* **2011**, *44*, 1281−1284.
(30) Morrison, G.; zur Loye, H.-C. Simple Correction for the Sample Shape and Radial Offset Effects on SQUID Magnetometers: Magnetic Measurements on Ln_2O_3(Ln=Gd, Dy, Er) Standards. *J. Solid State Chem.* **2015**, *221*, 334−337.
(31) Kubelka, P.; Munk, F. F. Ein Beittrag zur Optik der Farbanstriche. *Z. Technol. Phys.* **1931**, 593.
(32) Kurtz, S. K.; Perry, T. T. A Powder Technique for the Evaluation of Nonlinear Optical Materials. *J. Appl. Phys.* **1968**, *39*, 3798−3813.
(33) Ok, K. M.; Chi, E. O.; Halasyamani, P. S. Bulk characterization methods for non-centrosymmetric materials: second-harmonic generation, piezoelectricity, pyroelectricity, and ferroelectricity. *Chem. Soc. Rev.* **2006**, *35*, 710−717.
(34) Hatscher, S. T. U.; Synthese, W. Und Kristallstrukturen Von $Ln_3I(SiS_4)_2$ (LN=Pr, Nd, Sm, Tb). *Z. Anorg. Allg. Chem.* **2001**, *627*, 2198.

(35) Hatscher, S. T.; Urland, W. Synthesis and structures of chloride thiosilicates with lanthanides $Ln_3Cl[SiS_4]_2$ (Ln = La, Ce, Pr). *Mater. Res. Bull.* **2002**, *37*, 1239−1247.
(36) Vleck, V.; Hasbrouck, J. *The Theory of Electric and Magnetic Susceptibilities*; Oxford University Press, 1965.
(37) Misawa, Y.; Yoshihiro, D.; Yukio, H. Crystal structures and magnetic properties of ternary sulfides $BaLn_2S_4$ (Ln = Sm, Gd-Lu). *J. Ceram. Soc. Japan.* **2009**, *117*, 85−88.
(38) Shi, Y.-F.; Chen, Y.-k.; Chen, M.-C.; Wu, L.-M.; Lin, H.; Zhou, L.-J.; Chen, L. Strongest Second Harmonic Generation in the Polar R_3MTQ_7Family: Atomic Distribution Induced Nonlinear Optical Cooperation. *Chem. Mater.* **2015**, *27*, 1876−1884.
(39) Poduska, K. M.; DiSalvo, F. J.; Min, K.; Halasyamani, P. S. Structure determination of La_3CuGeS_7 and $La3_{Cu}GeSe_7$. *J. Alloys Compd.* **2002**, *335*, L5−L9.
(40) Yang, Y.; Chu, Y.; Zhang, B.; Wu, K.; Pan, S. Unique Unilateral-Chelated Mode-Induced d−p−π Interaction Enhances Second-Harmonic Generation Response in New Ln_3LiMS_7 Family. *Chem. Mater.* **2021**, *33*, 4225−4230.

https://doi.org/10.1021/acs.inorgchem.3c00708
Inorg. Chem. 2023, 62, 7446−7452